

Article

Volcanic Plume CO₂ Flux Measurements at Mount Etna by Mobile Differential Absorption Lidar

Simone Santoro ^{1,2}, Stefano Parracino ^{2,3}, Luca Fiorani ², Roberto D'Aleo ¹, Enzo Di Ferdinando ², Gaetano Giudice ⁴, Giovanni Maio ^{5,†}, Marcello Nuvoli ² and Alessandro Aiuppa ^{1,4,*}

¹ Dipartimento di Scienze della Terra e del Mare, Università di Palermo, 90123 Palermo, Italy; simone.santoro@unipa.it (S.S.); roberto.daleo01@unipa.it (R.D.)

² Nuclear Fusion and Safety Technologies Department, ENEA (Italian National Agency for New Technologies, Energy and Sustainable Economic Development), 00044 Frascati, Italy; stefano.parracino@uniroma2.it (S.P.); luca.fiorani@enea.it (L.F.); enzo.diferdinando@enea.it (E.D.F.); marcello.nuvoli@enea.it (M.N.)

³ Department of Industrial Engineering, University of Rome "Tor Vergata", 00173 Rome, Italy

⁴ Istituto Nazionale di Geofisica e Vulcanologia, 90146 Palermo, Italy; gaetano.giudice@ingv.it

⁵ ARES Consortium, 00100 Rome, Italy; prof.maio@gmail.com

* Correspondence: alessandro.aiuppa@unipa.it

† Current address: Vitrociset SpA, 00156 Rome, Italy.

Academic Editors: Andrew McGonigle, Giuseppe Salerno and Jesús Martínez-Frías

Received: 23 January 2017; Accepted: 27 February 2017; Published: 3 March 2017

Abstract: Volcanic eruptions are often preceded by precursory increases in the volcanic carbon dioxide (CO₂) flux. Unfortunately, the traditional techniques used to measure volcanic CO₂ require near-vent, in situ plume measurements that are potentially hazardous for operators and expose instruments to extreme conditions. To overcome these limitations, the project BRIDGE (BRIDging the gap between Gas Emissions and geophysical observations at active volcanoes) received funding from the European Research Council, with the objective to develop a new generation of volcanic gas sensing instruments, including a novel DIAL-Lidar (Differential Absorption Light Detection and Ranging) for remote (e.g., distal) CO₂ observations. Here we report on the results of a field campaign carried out at Mt. Etna from 28 July 2016 to 1 August 2016, during which we used this novel DIAL-Lidar to retrieve spatially and temporally resolved profiles of excess CO₂ concentrations inside the volcanic plume. By vertically scanning the volcanic plume at different elevation angles and distances, an excess CO₂ concentration of tens of ppm (up to 30% above the atmospheric background of 400 ppm) was resolved from up to a 4 km distance from the plume itself. From this, the first remotely sensed volcanic CO₂ flux estimation from Etna's northeast crater was derived at ≈2850–3900 tons/day. This Lidar-based CO₂ flux is in fair agreement with that (≈2750 tons/day) obtained using conventional techniques requiring the in situ measurement of volcanic gas composition.

Keywords: volcanic plumes; volcanic CO₂ flux; remote sensing; Differential Absorption Lidar (DIAL)

1. Introduction

In the last two decades, there have been major advances in the instrumental monitoring of volcanic gas plume composition and fluxes [1]. These have included the first instrumental networks of scanning Differential Optical Absorption Spectrometers (DOAS) for volcanic SO₂ flux monitoring, the implementation of satellite-based volcanic gas observations, and the advent of sensor units for in situ gas monitoring [1–6]. Owing to this technical progress, volcanic gas plume composition and fluxes have increasingly been used to extract information on degassing mechanisms/processes [4], and to derive constraints on shallow volcano plumbing systems [5]. However, work still needs to be done to increase the number of volcanic gas species that can be detected in plumes, which remain few if compared to the countless number of chemicals quantified from fumarole direct sampling [1].

Studying volcanic gas plumes has additionally contributed to monitoring, and eventually allowed the prediction of volcano behavior [6]. In particular, it has been shown that, at open-vent persistently degassing volcanoes, volcanic eruptions are often preceded by anomalous increases of the volcanic CO₂ flux [7]. These initial observations have motivated attempts to systematically monitor the volcanic CO₂ flux, and to identify novel measurement strategies [8]. Until recently, however, attempts to remotely sense the volcanic CO₂ flux from distal locations have been limited in number [9,10], while the majority of the observations have involved in situ measurements in the proximity of hazardous active volcanic vents [3]. On Mt. Etna, for example, one of the largest volcanic CO₂ point sources on Earth [11], the volcanic CO₂ flux has systematically been measured since the mid-2000s by combining in situ measurement of the volcanic CO₂/SO₂ ratio (with portable or permanent Multi-Component Gas Analyzer Systems, Multi-GAS; [12–15]) with remotely sensed SO₂ fluxes [16–18]. No successful report exists, at least to the best of our knowledge, of spectroscopy-based detection of Etna's volcanic CO₂ flux from a remote (distal) location.

Within the context of the ERC (European Research Council) starting the grant project BRIDGE (BRIDging the gap between Gas Emissions and geophysical observations at active volcanoes), we designed a new DIAL (Differential Absorption Lidar) [19], with the specific objective to remotely sense the volcanic CO₂ flux. Lidars have only recently been introduced in volcanic gas studies. A CO₂ laser-based lidar was used at Mt. Etna in 2008 [20] and at Stromboli Volcano in 2009 [21] to measure the volcanic plume water vapor flux. More recently, lidars were first used to target volcanic CO₂ [9,10,22–24]. Our lidar BILLI (BRIDGE volCANIC LIidar) [22], for example, has recently been used to successfully retrieve three-dimensional tomographies of volcanic CO₂ in the plumes of Pozzuoli, Solfatara in 2014 [9] and Stromboli volcano in 2015 [23,24]. As such, although gas-sensing lidars remain far less exploited in volcanology than those targeting volcanic ash/particles [25,26], this novel application field may expand rapidly in the near future.

Here, we report on the first successful use of BILLI at Mt. Etna. We show that, in our July–August 2016 Etna experiment, the lidar successfully resolved a volcanic CO₂ signal of a few tens of ppm (in excess to the background air) from more than 4 km of distance, and with good spatial (5 m) and temporal (10 s) resolution. These results are used to derive the first “remote” assessment of Etna's volcanic CO₂ flux. Our observations open new perspectives for routine volcanic CO₂ flux monitoring via lidars.

2. Materials and Methods

2.1. Field Set-Up on Mt. Etna

Observations on Mt. Etna were conducted from 28 July to 1 August 2016, including an initial phase of instrumental setup (28–29 July). Successful CO₂ flux detections were obtained on 31 July, when optimal viewing conditions persisted over the day. The DIAL was mounted in a trailer loaded on a truck, parked at the INGV (Istituto Nazionale di Geofisica e Vulcanologia) observatory “Pizzi Deneri” (Figure 1). The observatory is located at 2823 m a.s.l., northeast of the summit crater of Mt. Etna (3329 m a.s.l.), and at about 3 km from the main degassing vents (Figure 1).

The lidar was used to scan the volcanic plume vertically, keeping a constant azimuth angle (230°) and varying the elevation angle from 7° to 14° (Figure 1). A full 7° to 14° vertical scan was completed in ~15 min, and one atmospheric profile every 10 s was recorded throughout. With this instrumental set-up, the volcanic gas plume of the Etna's northeast crater was investigated (Figure 1), plumes from other craters being either too dilute (southeast crater) or only partially visible (central craters).

At our measurement conditions, two rock surfaces, corresponding to the eastern, outer flanks of the central crater, were intercepted by the laser beam at distances of 1.6 and 2.1 km, and at elevation angles from 7° to 9°. These rock surfaces retro-reflected the laser beam, yielding strong return signals (see below, Figure 2). The volcanic plume, e.g., high in-plume excess CO₂ concentrations, was detected in between the two above rock surfaces, and in the 2.2–4.2 km distance range.

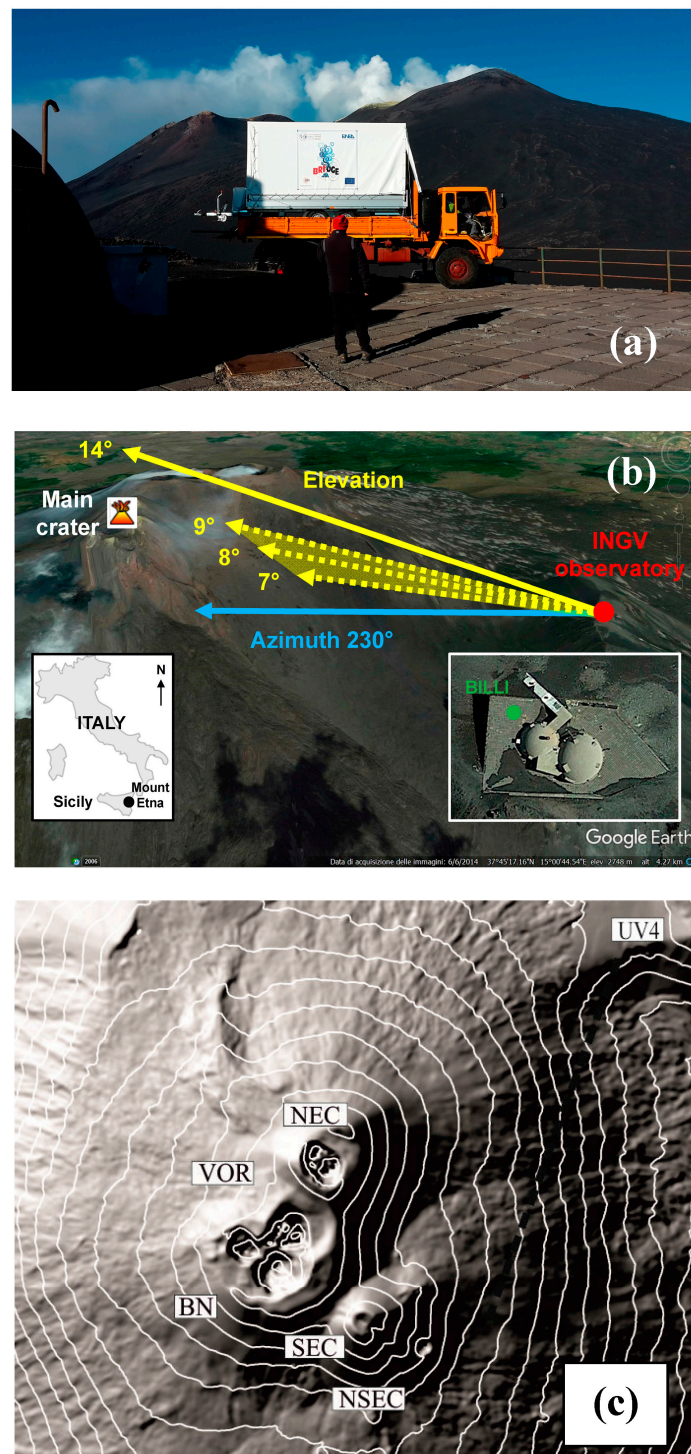


Figure 1. (a) The BILLI DIAL (BrIdge voLcanic Lidar, Differential Absorption Lidar) system mounted in a trailer (white) loaded on a truck (orange) at the INGV (Istituto Nazionale di Geofisica e Vulcanologia) observatory “Pizzi Deneri” (the volcanic plume of Mt. Etna is clearly visible); (b) Location of Mt. Etna in Sicily, southern Italy (left inset); the truck was parked at the INGV observatory “Pizzi Deneri” (right inset); the laser was fired at constant azimuth and different elevations. The volcanic plume of the northeast crater has been crossed by the laser beam. From 7° to 9° of elevation, rock faces were encountered; (c) A map of the summit area showing the active craters and the UV camera site (UV4). NEC: northeast crater; VOR: Voragine; BN: Bocca Nuova (VOR and BN are part of the Etna’s central craters); SEC: southeast crater; NSEC: new southeast crater.

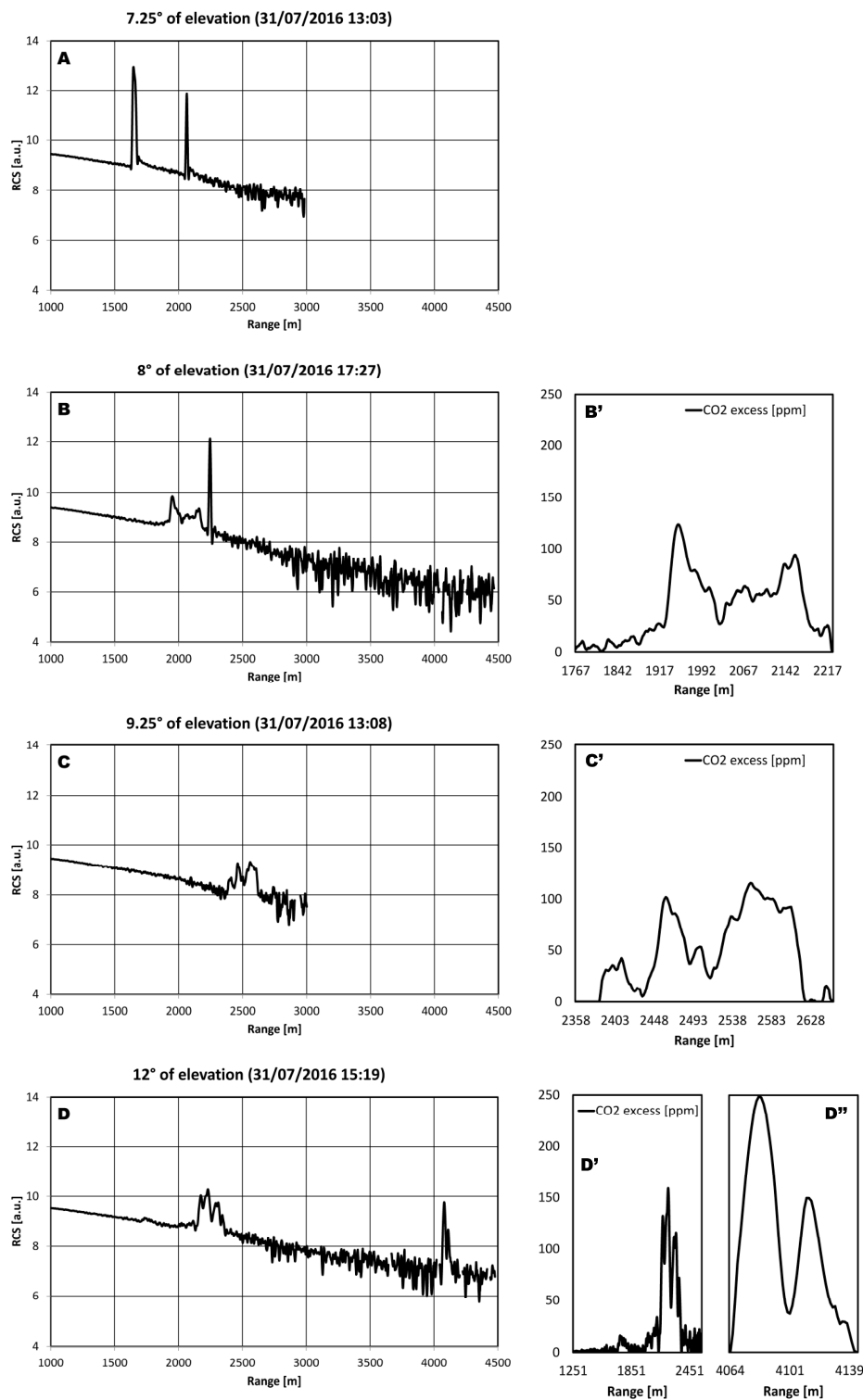


Figure 2. (A) Lidar return at 7.25° of elevation: two narrow and defined peaks due to beam backscattering from rock faces are clearly visible (beyond 3000 m only noise was recorded and the corresponding signal is not shown); (B) lidar return at 8° of elevation: a wide and jagged peak from the volcanic plume and a narrow and defined peak from a rock face are clearly visible; the CO₂ profile inside the volcanic plume is shown in (B'); (C) lidar return at 9.25° of elevation: a wide and jagged peak from the volcanic plume is clearly visible; the CO₂ profile inside the volcanic plume is shown in (C') (beyond 3000 m only noise was recorded and the corresponding signal is not shown); (D) lidar return at 12° of elevation: two wide and jagged peaks from the volcanic plume are clearly visible; the CO₂ profiles inside the volcanic plume are shown in (D',D'').

2.2. DIAL

The main components of a lidar are the transmitter (laser) and the receiver (telescope). A lidar is merely an optical radar [19]: a laser pulse is transmitted to the atmosphere, and some of its photons are backscattered to the telescope by air molecules and aerosols (droplets, particles etc.). The optical power corresponding to this photon flux is transformed into an electronic signal by photodetector and preamplifier, and converted in digital signal by an ADC (analog-to-digital converter).

The chemo-physical properties of the atmosphere along the laser beam, at distance R (range) from the lidar, can be inferred from analysis of the detected signal as a function of t , the time interval between emission and detection. R and t are linked by the relation $R = ct/2$, where c is the speed of light. The returned signal to the lidars' telescope, as a function of R (or t), then yields an atmospheric profile (Figure 2). In other words, an atmospheric profile is a range-resolved characterization of the lidar returned signal, which allows studying the air/plume optical properties along the light trajectory.

Air attenuates the laser pulse due to molecules and aerosol scattering and to the specific absorption of gases: if the laser wavelength coincides with absorption lines of a target gas, the attenuation will be stronger. A DIAL takes advantage of this effect: unlike a usual lidar, two wavelengths, ON and OFF, are transmitted, with only the former being absorbed by the target gas (Figure 3).

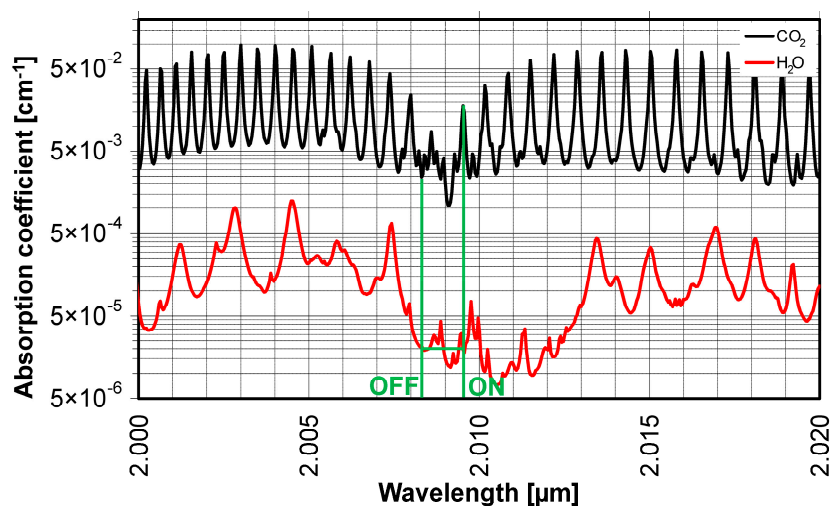


Figure 3. Carbon dioxide and water vapor absorption coefficients (from [27]) around the ON and OFF wavelengths (indicated in green).

If the absorption line is narrow, and ON and OFF wavelengths are close enough, the target gas concentration along the lidar optical path can be derived from the ratio between the OFF and ON signals. In this application, we selected the following wavelengths (Figure 3): ON, 2009.537 nm; OFF, 2008.484 nm. This selection was motivated by: (i) the CO_2 absorption is relatively low, thus allowing the system to probe far ranges (beyond 4 km). If a stronger line had been used, the ON laser pulse would have extinguished before; (ii) the beam energy (depending mainly on the dye efficiency curve) and the detector responsivity are near their maximum; and (iii) the H_2O absorption is very low (Figure 3). Moreover, ON and OFF have been chosen so that the differential absorption of H_2O is approximately zero (within the uncertainty of the spectroscopic data), thus minimizing the interference of water vapor to the carbon dioxide measurement.

In our case, the transmitter and the receiver are coaxial, and the lidar field-of-view can be aimed in the whole atmosphere thanks to a system made of two large elliptical mirrors [22]. This configuration allows the experimenters to scan the plume in both horizontal and vertical planes, thus measuring CO_2 concentrations both outside and inside the volcanic plume [9]. From this, by scanning the volcanic gas plume from different angles and viewing directions, the CO_2 distribution in a cross-section of the

volcanic plume can be retrieved. This, combined with independent knowledge of plume speed and altitude, allows the CO₂ flux to be retrieved.

The reader is referred to previous work [9,22–24] for details on instrumental setup and data processing. The systematic error associated with the derived CO₂ concentrations is dominated by imprecision in wavelength setting [22]. This leads to inaccuracy in the differential absorption cross section, and thus in gas concentration. Thanks to a photo-acoustic cell filled with pure CO₂ at atmospheric pressure and temperature, the ON and OFF wavelengths were set before each atmospheric scan. The residual imprecision [23] of $\pm 0.02 \text{ cm}^{-1}$ (half laser linewidth: half width at half maximum of the energy transmitted by the laser system (J) vs the wavenumber (cm^{-1})) implies a systematic error on CO₂ concentrations of 5.5% [24]. The statistical error of CO₂ measurement has been calculated by usual error propagation techniques from the standard deviation of the lidar signal. At 2.5 km, a mean range, it is about 2%, while it can exceed 5% at 4.2 km. Table 1 compares the instrumental set-up during the Mt. Etna field campaign, with those used at Solfatara [9,22], and Stromboli [23,24].

Table 1. Summary of field operational conditions at Pozzuoli Solfatara, Stromboli, and Mt. Etna (this study).

Campaign	Pozzuoli Solfatara	Stromboli Volcano	Mt. Etna
Latitude	40°49'46.28"N	38°48'06.69"N	37°45'57.28"N
Longitude	14°08'50.51"E	15°14'25.69"E	15°00'59.65"E
Period	13–17 October 2014	24–29 June 2015	28 July–1 August 2016
Azimuth scan	196°–234°	235.3°–253.6°	230°
Elevation scan	0°–18°	15.2°–27.4°	7°–14°

3. Results

Figure 2 shows examples of lidar returns obtained during our Etna campaign. Results are illustrated for four atmospheric profiles taken on 31 July (the best measurement day) at four distinct elevations, and are shown in the form of range vs. RCS (range corrected signal) scatter plots.

During its atmospheric propagation, the laser beam intensity approximately decreased:

- exponentially, due to atmospheric extinction, according to the Lambert-Beer law, and;
- as $1/R^2$, because the solid angle subtended by the receiver is A/R^2 , where A is the telescope effective area.

For these reasons, it is a common practice in lidar science to express results using a RCS, this being the logarithm of the product of the signal times the square of the range. To improve the SNR (signal-to-noise ratio), the RCS was obtained by averaging 50 laser shots for each lidar return, and a 13-point Savitzky-Golay filter was applied [28].

During a vertical scan, the measured range-resolved RCS profiles varied as the laser elevation was sequentially increased. Below 7.25° elevation, the laser beam hit a first rock surface at about a 1.6 km distance. Laser beam retro-reflection at this rock surface produced, in the lidar return signal, a strong, narrow RCS peak at $R = 1.6$ km. At 7.25° elevation (Figure 2a), only part of the beam was intercepted by the $R = 1.6$ km rock surface, while the remaining part impinged on the rock surface at $R = 2.1$ km, producing a second narrow RCS peak. For geometrical reasons, an elevation increase corresponded to an increase in the range at which the rock surfaces were encountered, e.g., the second rock surface was encountered at $R = 2.1$ at 7.25° elevation, shown in Figure 2a, and at $R = 2.3$ km at 8° elevation, shown in Figure 2b. No rock surface was hit by the laser beam at elevations $>9^\circ$, e.g., note the absence of narrow RCS peaks in Figure 2c,d.

Back-scattering of the laser beam by the volcanic plume produced wide and jagged RCS peaks, therefore very distinct from the narrow and defined peaks produced by beam retro-reflection at rock surfaces (compare the two peak shapes in Figure 2b).

The volcanic plume was detected at range distances in between the two rock surfaces up to a 9° elevation (e.g., Figure 2b), or beyond them at a 9° to 14° elevation (Figure 2c,d). A broad, irregular RCS peak in the lidar returns, corresponding to the volcanic plume, was resolved up to a maximum measurement range of 4.2 km (Figure 2d).

We used the procedure detailed in References [9,24] to convert the RCS profiles into range-resolved profiles of in-plume excess CO₂ concentrations (see Figure 2b',c',d',d''). This procedure involves calculating the excess CO₂ concentration corresponding to each *i*-th ADC channel of the lidar profile from:

$$C_{\text{CO}_2,i} = k \text{RCS}_i \quad (1)$$

$$k = \frac{\Delta C (R_1 - R_2)}{\Delta R \sum_i \text{RCS}_i} \quad (2)$$

where ΔR and RCS_i are, respectively, the range interval and range corrected signal corresponding to each ADC channel; R_1 and R_2 are the range distances of the two above rock surfaces; and ΔC is the average excess CO₂ concentration in the air/plume parcel between them (this is obtained from the intensity contrast of lidar returns produced by the two rock surfaces). The term “excess” implies that the reported CO₂ concentrations are after subtraction of the ambient atmospheric background, and therefore correspond to the “volcanic” CO₂ levels in the plume. The ambient atmospheric CO₂ background was obtained from the processing of lidar returns in the 0–1.6 km range distance, where no plume signal was detected (see Reference [9] for details of calculations).

At an 8° elevation, shown in Figure 2b', the volcanic plume was evidenced by a band of excess CO₂ concentrations of ≤125 ppm. These excess CO₂ concentrations agree well with those derived by in situ in-plume measurements with conventional techniques (e.g., the Multi-GAS), from which in-plume CO₂ concentrations of tens to hundreds of ppm above ambient air are typically obtained [12]. The plume appears to be about 300 m thick; this relatively narrow plume's cross-section was probably justified by the fact that, at such an 8° elevation, the laser beam intercepted the volcanic plume at below the summit crater's rim altitude. Due to its close proximity to the crater slopes, the volcanic plume was, at least partly, protected from the local wind field, a fact that reduced its atmospheric dispersion. The volcanic plume was still relatively narrow at a ~9° elevation (Figure 2c'), where the laser beam pointed just above the summit crater's rim. At even higher elevations, the volcanic plume was wider and scattered by the wind, and the returned RCS often presented multiple peaks (Figure 2d,d').

As explained before (Section 2), a sequence of atmospheric profiles was acquired as the lidar vertically scanned the horizon, from a 7° to 14° (max) elevation. All CO₂ profiles (e.g., Figure 2), taken at different elevations during a single lidar rotation sequence, were combined and integrated to obtain a CO₂ scan, examples of which are illustrated in Figure 4. On 31 July 2016, the most fruitful day, 19 scans were obtained. Each scan consisted of 24 profiles, all at a 230° azimuth. These profiles covered the elevation angle interval (between 7° and 13°) with an angular resolution of about 0.25°.

The results are illustrated in the form of contour maps of excess CO₂ concentrations, plotted as a function of the range and elevation. The colored spots correspond to areas of high excess CO₂ (the natural background is dark blue), and therefore illustrate the spatial distribution and temporal evolution of the volcanic plume (the yellow lines delimit the positions of the laser beam reflections off the rock surfaces). In all the maps we obtained (see examples in Figure 4), the structure of the plume was well resolved. The plume was tracked as a cluster of high CO₂ concentration spots, trending from about a 9° elevation and $R = 2.4$ km (the vent rim) to a 13° elevation and $R = 2.5$ – 2.9 km. As such, our CO₂ concentration maps were consistent with a gently lofting volcanic plume (Figure 4), with vertical and horizontal movements driven by thermal buoyancy and by the local wind field pattern. The maps indicate the plume was being dispersed away from the lidar during our observations, since the range of volcanic plume detection increased with the elevation in all the maps.

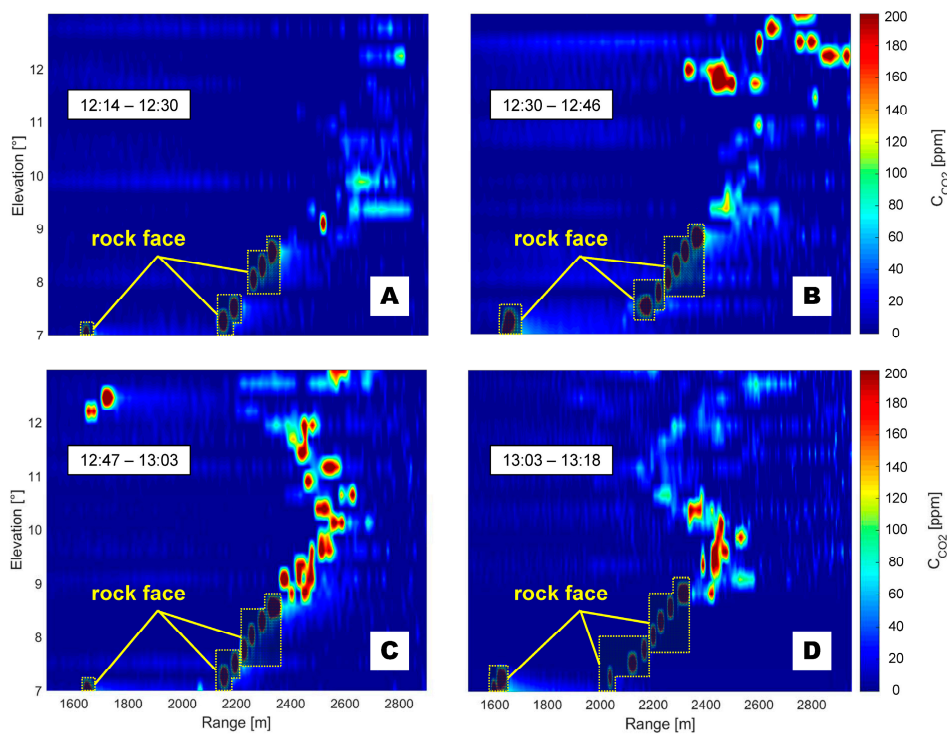


Figure 4. Vertical scans (fixed azimuth: 230°) of the volcanic plume (CO₂ excess) acquired on 31 July 2016; (A) from 12:14 p.m. to 12:30 p.m.; (B) from 12:30 p.m. to 12:46 p.m.; (C) from 12:47 p.m. to 1:03 p.m. and (D) from 1:03 p.m. to 1:18 p.m. (local civil time). At this azimuth, in the elevation interval between 7° and 9°, the laser beam is back-scattered by rock faces, thus causing signal peaks not due to the volcanic plume (rock faces are sorted out from real CO₂ by the correspondence of narrow peaks with certain range values).

The maps of Figure 4 set the basis for the calculation of the volcanic CO₂ flux. In analogy with previous work [9], we obtained the volcanic CO₂ flux by integrating the background-corrected (excess) CO₂ concentrations over a plume cross-section (from the maps of Figure 4), which allowed us to derive the plume CO₂ molecular density. This was then multiplied by the plume transport speed to obtain the CO₂ flux (Φ_{CO_2} , in Kg·s⁻¹), as:

$$\Phi_{CO_2} = v_p \cdot \frac{PM_{CO_2}}{10^3 N_A} \cdot N_{molCO_2-total} \quad (3)$$

where v_p is the plume transport speed (in m/s); $N_{molCO_2-total}$ is the total-plume CO₂ molecular density (expressed in molecules·m⁻³); and PM_{CO_2} and N_A are, respectively, the CO₂ molecular weight and Avogadro's constant. The term $N_{molCO_2-total}$ was obtained by integrating the effective average excess CO₂ concentrations ($\overline{C_{exc,i}}$ [ppm]) over the entire plume cross-section, according to:

$$N_{molCO_2-total} = N_h \cdot 10^{-6} \cdot \sum_i \overline{C_{exc,i}} \cdot A_i \quad (4)$$

where N_h is the atmospheric number density (molecules·m⁻³) at the crater's summit height, and A_i represents the i-th effective plume area.

The plume transport speed was inferred at 9.7 ± 0.8 m/s from the processing of plume images taken on the same day by the permanent UV camera system (UV4) in use at the Pizzi Deneri observatory since 2014; see Reference [29] for details on the instrument. The UV camera images were processed using an optical flow sub-routine using the Lukas/Kanade algorithm [30,31], integrated in the Vulcamera software [32] (same methodology as described in [29]).

Our derived CO₂ fluxes are illustrated in Figure 5. The CO₂ flux varied from 1235 to 8050 tons/day during the measurement interval, and averaged at 2850 ± 1800 tons/day.

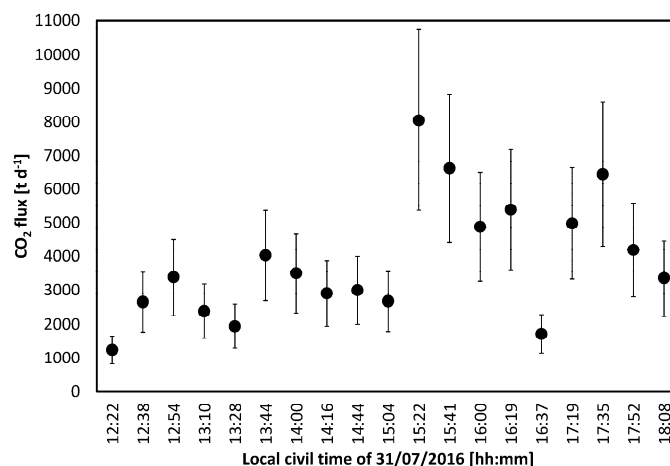


Figure 5. CO₂ flux from the northeast crater retrieved on 31 July 2016 from 12:22 p.m. to 6:08 p.m. (local civil time). The error bars indicate the inferred CO₂ flux error (±33%), as based upon the error propagation of the plume speed and in-plume integrated CO₂ amounts (procedure detailed in [24]).

4. Discussion

As long-term volcanic gas records have increased in number and quality over the last few decades [33], full empirical evidence has emerged for precursory increases of the volcanic CO₂ flux emissions prior to eruption of mafic to intermediate volcanoes [7]. However, remote direct measurements of the volcanic CO₂ flux, which are intrinsically safer for operators and more prone to provide continuous, long-term observations, have remained impossible until recently [9,10].

Our results here support the ability of the DIAL-Lidar BILLI to profile atmospheric CO₂ concentrations over large optical paths (Figures 2 and 4), and to remotely sense the CO₂ flux from distal (up to 4 km distant) sources (Figure 5). This instrument thus promises a real step ahead in the remote observation of volcanic gas emissions. Improved CO₂ flux measurements are not only vital for better gas-based volcano monitoring, but are also needed to better constrain the global volcanic CO₂ budget, which is still inaccurately known [8].

The volcanic CO₂ flux from Mt. Etna has been assessed in the past by either in-plume airborne CO₂ profiling [11], or by indirect methods involving in situ measurements of plume CO₂/SO₂ ratios, via either the Multi-GAS [3,12–15] or Fourier Transform InfraRed Spectrometers (FTIR; [16]). To the best of our knowledge, our results are the first to report a direct, remote quantification of Etna's CO₂ flux.

Our lidar results show that, in the circa 5-h-long observational window, the CO₂ flux from Etna's northeast crater varied from 1235 to 8050 tons/day (Figure 5). The CO₂ flux was somewhat higher, typically >4000 tons/day and up to 8050 tons/day, after 3 p.m. local time, relative to the 12–3 p.m. period (<4000 tons/day) (Figure 5). No change in activity was yet observed at the northeast crater, which continued to exhibit quiescent degassing over the entire measurement interval. We therefore consider the observed variation as part of the normal fluctuations in degassing activity that occur at Etna, likely in response to temporal variations in the magma/gas transport rate in the volcano's feeding conduits [15–18]. By taking the arithmetic mean of the individual CO₂ flux measurements in Figure 5, we would obtain a time-averaged CO₂ flux of 2850 ± 1800 tons/day for 31 July 2016. In view of the non-stationary CO₂ emission behavior captured by our high-temporal resolution measurement (Figure 5), we also perform an independent exercise in which we calculated the total CO₂ output from the northeast crater by integrating (in the time domain) the available CO₂ flux measurements, each representative of 13–18 min of observation (the mean duration of scans was

15 min). From this, we obtained that ≈ 796 tons of CO_2 were cumulatively released during 5 h of observations, implying a time-averaged CO_2 flux of 3900 tons/day. This is about 30% higher than, but within one standard deviation of, the CO_2 flux obtained above from a simple arithmetic mean approach (2850 ± 1800 tons/day).

In the attempt to add confidence to our results, we compared our lidar-based CO_2 flux with independent estimates based upon a more conventional technique that involves a combination of SO_2 fluxes and plume CO_2/SO_2 ratios (Figure 6). Our permanent UV camera system (UV4) at Pizzi Deneri indicated, for the morning of the same 31 July, a time-averaged SO_2 flux of 645 ± 125 tons/day. This is the mean (± 1 standard deviation) of 4 h of observations at a 0.5 Hz rate (Figure 6; same methodology as in [29]). Our inferred northeast crater's SO_2 flux (645 ± 125 tons/day) corresponded to about 30% of the total volcano's SO_2 emissions (≈ 2200 tons/day). These latter emissions were inferred using the same UV camera system, and were thus primarily determined by the central craters (not targeted by our DIAL-Lidar). The northeast crater's volcanic plume was in situ measured by a portable Multi-GAS instrument (the same as in [12,13]) two days later. These in situ observations yielded a (molar) CO_2/SO_2 ratio of ≈ 6 , demonstrating the usual [12,16] CO_2 -poor composition of the northeast crater (the simultaneously observed CO_2/SO_2 ratio of the central crater's plume was ≈ 16). We consider our Multi-GAS-derived composition on 2 August as still representative of the northeast crater's emissions on 31 July, since volcanic activity at that crater did not exhibit any substantial change in between the two days. By combining the two sets of data together, we converted the SO_2 flux time-series into a 4-h-long CO_2 flux time-series (Figure 6), from which an averaged (arithmetic mean) UV-Camera + MultiGAS CO_2 flux of ≈ 2750 tons/day was obtained. This is close to our lidar-based estimates above (≈ 2850 – 3900 tons/day). We caution that the two independent CO_2 flux time-series (from lidar and UV-Camera + MultiGAS) are not temporally overlapping, since the UV camera system ran only in the morning, when sunlight conditions were optimal [29], while our successful CO_2 flux measurement with the lidar started a few hours later in the afternoon. In addition, the UV-Camera + MultiGAS used a constant CO_2/SO_2 ratio (of six) throughout the entire UV camera temporal window, while it is valid only as a first approximation. However, the close CO_2 flux values inferred from lidar and UV-Camera + MultiGAS provide mutual validation for the two independent techniques.

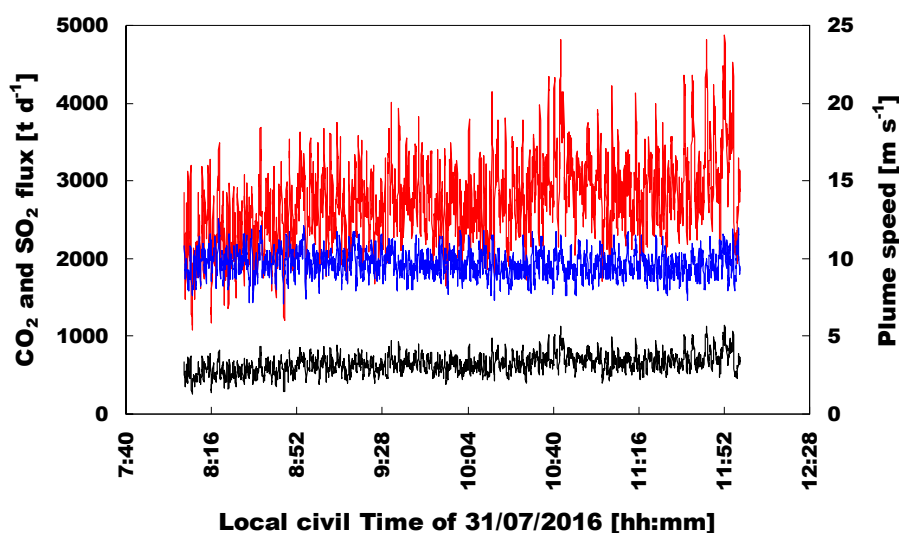


Figure 6. Time-series of CO_2 flux emissions from the northeast crater (in red) obtained from the UV-Camera + Multi-Gas technique. These were calculated by converting the SO_2 flux time-series (in black) obtained by the UV4 permanent UV camera system on 31 July 2016 (from 8 a.m. to 12 p.m., local civil time) using a CO_2/SO_2 ratio (molar) of six. The plume speed time-series calculated from the UV camera on the same 31 July is also shown (blue trend).

5. Conclusions

We have shown for the first time that the volcanic CO₂ flux can be detected with lidar from up to a 4 km distance. During our Mt. Etna field campaign, our DIAL-Lidar BILLI vertically scanned the volcanic plume while profiling CO₂ concentrations every 10 s, with a spatial resolution of 5 m. With this configuration, we successfully detected an excess volcanic CO₂ signal of a few tens of ppm, with relatively low systematic and statistical errors (5.5% and 2%, respectively). By integrating the results of the atmospheric profile taken at different heading angles, and covering a full scan of the plume, the volcanic CO₂ flux was derived (after integration, and in combination with the plume transport speed) at ≈2850–3900 tons/day. This lidar-based flux is close to that independently obtained by in situ observations of the volcanic plume (≈2750 tons/day), which combined Multi-GAS in situ sensing of the plume composition and remotely sensed (UV camera) SO₂ fluxes.

Clearly, additional field tests are required to validate our novel technique even further. Still, our results suggest BILLI is a major advance in ground-based observations of volcanic plumes. The instrument allows the remote measurements of volcanic CO₂ (and particles, if desired) from distal (safe) areas, and with unprecedented temporal resolution and high spatial coverage. Further development is now required to make this technology an operational tool for routine volcanic gas observations. Efforts are currently being undertaken to reduce the weight and power requirements (the current prototype is ~1100 kg and requires 6.5 kW), and to implement more user-friendly operational routines and software. These implementations are required to widen the application range of the lidar, and to allow its use in remote/harsh volcanic environments.

Acknowledgments: The authors are grateful to ENEA, in general, and Aldo Pizzuto, Roberta Fantoni and Antonio Palucci, in particular, for constant encouragement. They thank the staff of INGV-OE, and especially the Director Eugenio Privitera and Salvatore Consoli, for logistical support and for granting access to the INGV observatory “Pizzi Deneri”. The support from the ERC project BRIDGE, n. 305377, is gratefully acknowledged. This work benefitted from the insightful comments of two anonymous reviewers.

Author Contributions: S.S., L.F. and A.A. conceived and designed the experiments; S.S., L.F., R.D., E.D.F., M.N., G.G., and A.A. performed the experiments; S.P., G.M., and R.D. analyzed the data; A.A., L.F. and S.S. wrote the paper with contributions from all co-authors.

Conflicts of Interest: The authors declare no conflict of interest.

References

1. Oppenheimer, C.; Fischer, T.P.; Scaillet, B. Volcanic Degassing: Process and Impact. In *Treatise on Geochemistry, The Crust*, 2nd ed.; Holland, H.D., Turekian, K.K., Eds.; Elsevier: Amsterdam, The Netherlands, 2014; Volume 4, pp. 111–179.
2. Carn, S.A.; Clarisse, L.; Prata, A.J. Multi-decadal satellite measurements of global volcanic degassing. *J. Volcanol. Geothermal Res.* **2016**, *311*, 99–134. [[CrossRef](#)]
3. Aiuppa, A. Volcanic gas monitoring. In *Volcanism and Global Environmental Change*; Schmidt, A., Fristad, K.E., Elkins-Tanton, L.T., Eds.; Cambridge University Press: Cambridge, UK, 2015; pp. 81–96.
4. Edmonds, M. New geochemical insights into volcanic degassing. *Philos. Trans. R. Soc. A Math. Phys. Eng. Sci.* **2008**, *366*, 4559–4579. [[CrossRef](#)] [[PubMed](#)]
5. Allard, P.; Carbonnelle, J.; Métrich, N.; Loyer, H.; Zettwoog, P. Sulphur output and magma degassing budget of Stromboli volcano. *Nature* **1994**, *368*, 326–330. [[CrossRef](#)]
6. Saccorotti, G.; Iguchi, M.; Aiuppa, A. In situ Volcano Monitoring: Present and Future. In *Volcanic Hazards, Risks and Disasters*; Elsevier: Amsterdam, The Netherlands, 2014; pp. 169–202.
7. Aiuppa, A.; Burton, M.; Caltabiano, T.; Giudice, G.; Guerrieri, S.; Liuzzo, M.; Murè, F.; Salerno, G. Unusually large magmatic CO₂ gas emissions prior to a basaltic paroxysm. *Geophys. Res. Lett.* **2010**, *37*, L17303. [[CrossRef](#)]
8. Burton, M.R.; Sawyer, G.M.; Granieri, D. Deep carbon emissions from volcanoes. *Rev. Mineral. Geochem.* **2013**, *75*, 323–354. [[CrossRef](#)]
9. Aiuppa, A.; Fiorani, L.; Santoro, S.; Parracino, S.; Nuvoli, M.; Chiodini, G.; Minopoli, C.; Tamburello, G. New ground-based lidar enables volcanic CO₂ flux measurements. *Sci. Rep.* **2015**, *5*, 13614. [[CrossRef](#)] [[PubMed](#)]

10. Queißer, M.; Granieri, D.; Burton, M. A new frontier in CO₂ flux measurements using a highly portable DIAL laser system. *Sci. Rep.* **2016**, *6*, 33834.
11. Allard, P.; Carbonnelle, J.; Dajlevic, D.; le Bronec, J.; Morel, P.; Robe, M.C.; Maurenas, J.M.; Faivre-Pierret, R.; Martin, D.; Sabroux, J.C.; et al. Eruptive and diffuse emissions of CO₂ from Mount Etna. *Nature* **1991**, *351*, 387–391. [[CrossRef](#)]
12. Aiuppa, A.; Federico, C.; Giudice, G.; Gurrieri, S.; Liuzzo, M.; Shinohara, H.; Favara, R.; Valenza, M. Rates of carbon dioxide plume degassing from Mount Etna volcano. *J. Geophys. Res.* **2006**, *111*, B09207. [[CrossRef](#)]
13. Aiuppa, A.; Giudice, G.; Gurrieri, S.; Liuzzo, M.; Burton, M.; Caltabiano, T.; McGonigle, A.J.S.; Salerno, G.; Shinohara, H.; Valenza, M. Total volatile flux from Mount Etna. *Geophys. Res. Lett.* **2008**, *35*, L24302. [[CrossRef](#)]
14. Patanè, D.; Aiuppa, A.; Aloisi, M.; Behncke, B.; Cannata, A.; Coltelli, M.; di Grazia, G.; Gambino, S.; Gurrieri, S.; Mattia, M.; et al. Insights into magma and fluid transfer at Mount Etna by a multiparametric approach: A model of the events leading to the 2011 eruptive cycle. *J. Geophys. Res. Solid Earth* **2013**, *118*, 3519–3539. [[CrossRef](#)]
15. Pering, T.D.; Tamburello, G.; McGonigle, A.J.S.; Aiuppa, A.; Cannata, A.; Giudice, G.; Patanè, D. High time resolution fluctuations in volcanic carbon dioxide degassing from Mount Etna. *J. Volcanol. Geotherm. Res.* **2014**, *270*, 115–121. [[CrossRef](#)]
16. La Spina, A.; Burton, M.; Salerno, G.G. Unravelling the processes controlling gas emissions from the central and northeast craters of Mt. Etna. *J. Volcanol. Geotherm. Res.* **2010**, *198*, 368–376. [[CrossRef](#)]
17. Caltabiano, T.; Burton, M.; Giammanco, S.; Allard, P.; Bruno, N.; Murè, F.; Romano, R. Volcanic Gas Emissions from the Summit Craters and Flanks of Mt. Etna, 1987–2000. In *Mt. Etna: Volcano Laboratory*; Bonaccorso, A., Calvari, S., Coltelli, M., del Negro, C., Falsaperla, S., Eds.; Geophysical Monograph Series; American Geophysical Union: Washington, DC, USA, 2004; Volume 143, pp. 111–128.
18. Allard, P.; Behncke, B.; D’Amico, S.; Neri, M.; Gambino, S. Mount Etna 1993–2005: Anatomy of an evolving eruptive cycle. *Earth-Sci. Rev.* **2006**, *78*, 85–114. [[CrossRef](#)]
19. Fiorani, L. Lidar application to lithosphere, hydrosphere and atmosphere. In *Progress in Laser and Electro-Optics Research*; Koslovskiy, V.V., Ed.; Nova: New York, NY, USA, 2010; pp. 21–75.
20. Fiorani, L.; Colao, F.; Palucci, A. Measurement of Mount Etna plume by CO₂-laser-based lidar. *Opt. Lett.* **2009**, *34*, 800–802. [[CrossRef](#)] [[PubMed](#)]
21. Fiorani, L.; Colao, F.; Palucci, A.; Poreh, D.; Aiuppa, A.; Giudice, G. First-time lidar measurement of water vapor flux in a volcanic plume. *Opt. Commun.* **2011**, *284*, 1295–1298. [[CrossRef](#)]
22. Fiorani, L.; Santoro, S.; Parracino, S.; Nuvoli, M.; Minopoli, C.; Aiuppa, A. Volcanic CO₂ detection with a DFM/OPA-based lidar. *Opt. Lett.* **2015**, *40*, 1034–1036. [[CrossRef](#)] [[PubMed](#)]
23. Fiorani, L.; Santoro, S.; Parracino, S.; Maio, G.; Nuvoli, M.; Aiuppa, A. Early detection of volcanic hazard by lidar measurement of carbon dioxide. *Nat. Hazards* **2016**, *83*, S21–S29. [[CrossRef](#)]
24. Aiuppa, A.; Fiorani, L.; Santoro, S.; Parracino, S.; D’Aleo, R.; Liuzzo, M.; Maio, G.; Nuvoli, M. Advances in Dial-Lidar-based remote sensing of the volcanic CO₂ flux. *Front. Earth Sci.* **2017**, *5*, 15. [[CrossRef](#)]
25. Scollo, S.; Boselli, A.; Coltelli, M.; Leto, G.; Pisani, G.; Spinelli, N.; Wang, X. Monitoring Etna volcanic plumes using a scanning LiDAR. *Bull. Volcanol.* **2012**, *74*, 2383–2395. [[CrossRef](#)]
26. Wanga, X.; Boselli, A.; D’Avino, L.; Pisani, G.; Spinelli, N.; Amodeo, A.; Chaikovsky, A.; Wiegner, M.; Nickovic, S.; Papayannis, A.; et al. Volcanic dust characterization by EARLINET during Etna’s eruptions in 2001–2002. *Atmos. Environ.* **2008**, *42*, 893–905. [[CrossRef](#)]
27. Rothman, L.S.; Gordon, I.E.; Babikov, Y.; Barbe, A.; Benner, D.C.; Bernath, P.F.; Birk, M.; Bizzocchi, L.; Boudon, V.; Brown, L.R.; et al. The HITRAN2012 molecular spectroscopic database. *J. Quant. Spectrosc. Radiat. Transf.* **2013**, *130*, 4–50. [[CrossRef](#)]
28. Schafer, R.W. What is a Savitzky-Golay Filter? *IEEE Signal Process Mag.* **2011**, *28*, 111–117. [[CrossRef](#)]
29. D’Aleo, R.; Bitetto, M.; Delle Donne, D.; Tamburello, G.; Battaglia, A.; Coltelli, M.; Patanè, D.; Prestifilippo, M.; Sciotto, M.; Aiuppa, A. Spatially resolved SO₂ flux emissions from Mt Etna. *Geophys. Res. Lett.* **2016**, *43*. [[CrossRef](#)] [[PubMed](#)]
30. Bruhn, A.; Weickert, J.; Schnörr, C. Lucas/Kanade Meets Horn/Schunck: Combining Local and Global Optic Flow Methods. *Int. J. Comput. Vis.* **2005**, *61*, 211–231. [[CrossRef](#)]
31. Peters, N.; Hoffmann, A.; Barnie, T.; Herzog, M.; Oppenheimer, C. Use of motion estimation algorithms for improved flux measurements using SO₂ cameras. *J. Volcanol. Geotherm. Res.* **2015**, *300*, 58–69. [[CrossRef](#)]

32. Tamburello, G.; Kantzas, E.P.; McGonigle, A.J.S.; Aiuppa, A. Vulcamera: A program for measuring volcanic SO₂ using UV cameras. *Ann. Geophys.* **2011**, *54*, 2. [[CrossRef](#)]
33. Fischer, T.P.; Chiodini, G. Volcanic, Magmatic and Hydrothermal Gas Discharges. In *Encyclopaedia of Volcanoes*, 2nd ed.; Elsevier: Amsterdam, The Netherlands, 2015; pp. 779–797.



© 2017 by the authors. Licensee MDPI, Basel, Switzerland. This article is an open access article distributed under the terms and conditions of the Creative Commons Attribution (CC BY) license (<http://creativecommons.org/licenses/by/4.0/>).